Outgoing excitonic resonance in resonant Raman scattering in a magnetic field

V. I. Belitskiĭ and A. Cantarero

Departmento de Física Aplicada, Universidad de Valencia, Burjasot, E-46100 Valencia, Spain

M. Cardona

Max Planck Institut für Festkörperforschung, D-70569 Stuttgart, Germany

I. G. Lang and A. V. Prokhorov

A. F. Ioffe Physicotechnical Institute, Russian Academy of Sciences, 194021 St. Petersburg, Russia

S. T. Pavlov

P. N. Lebedev Physics Institute, Russian Academy of Sciences, 117924 Moscow, Russia

(Submitted 12 February 1996)
Zh. Éksp. Teor. Fiz. **110**, 981–1000 (September 1996)

It is shown that the combined mechanism of multiphonon light scattering in polar semiconductors involving free electron–hole pair states (exciton states of the continuous spectrum) and exciton states of the discrete spectrum as intermediate states of the system leads to significant enhancement of the scattering efficiency in a strong magnetic field and to outgoing excitonic resonance. Taken separately, each of these mechanisms leads either to enhancement of the scattering efficiency in the presence of a strong magnetic field (in the case of free electron–hole pairs) or to outgoing excitonic resonance at the frequency of the exciton energy gap (in the case of discrete excitons). © *1996 American Institute of Physics.*
[S1063-7761(96)01709-X]

1. INTRODUCTION

The multiphonon resonant Raman spectra of bulk semiconductor compounds (CdS, CdSe, ZnO, ZnS, ZnSe, ZnTe, GaP, InAs, InBr, and InI) exhibit so-called outgoing excitonic resonance, i.e., an increase in the scattering intensity when the frequency of the scattered light $\omega_s=\omega_l-N\omega_{\rm LO}$ approaches the value $\omega_{\rm exc}$ that corresponds to the energy of the exciton ground state (ω_l is the frequency of the exciting light, $\omega_{\rm LO}$ is the frequency of longitudinal optical (LO) phonons, and N is the number of LO phonons emitted). Hence, it follows that the theory of multiphonon resonant Raman scattering should take into account the exciton states (of the discrete spectrum) as intermediate states in the light scattering process. However, a theory which utilizes only exciton states of the discrete spectrum predicts a rapid decrease in the scattering efficiency with increasing N, if the decay of these discrete exciton states with a transition to the continuum (exciton states of the continuous spectrum) is taken into account. Such a result, however, is not consistent with experiment, where up to 20 phonon replicas have been observed ($N=9$ for CdS, $N=20$ for InI and InBr).

Multiphonon resonant Raman scattering via exciton states of the discrete spectrum can be described as follows: an incident photon creates a hot Wannier–Mott exciton by means of an indirect transition with the emission of an optical (LO) phonon. Then the exciton successively emits $N-2$ LO phonons, decreasing its energy by $\hbar\omega_{\rm LO}$ in each step of the cascade process. The process ends with indirect recombination of the exciton accompanied by the emission of the last LO phonon and a quantum of secondary radiation $\hbar\omega_s$. The scattering cross section $\sigma_N^{\rm exc}$ for this process is proportional to the first power of the Fröhlich constant α of the electron–phonon interaction for arbitrary scattering order N. An increase in N by unity leads to the appearance of the factor $\gamma_s/\gamma_{\rm exc}$, where $\gamma_{\rm exc}\simeq\gamma_s+\gamma_d$ is the total reciprocal lifetime of the exciton, γ_d and γ_s are the probabilities of scattering into the continuum (exciton decay) and into a discrete state, respectively. It has been shown that when $m_e\ll m_h$, where m_e (m_h) is the electron (hole) effective mass, this factor amounts to $\gamma_s/\gamma_{\rm exc}\simeq 1/2$, while $\gamma_s/\gamma_{\rm exc}\ll 1$ when $m_e\simeq m_h$. The factors $\gamma_s/\gamma_{\rm exc}<1$ accumulate as N increases, and this should have resulted in a rapid decrease in the cross section $\sigma_N^{\rm exc}$. In such a case a theory of multiphonon resonant Raman scattering that takes into account only exciton states of the discrete spectrum as intermediate states cannot describe scattering processes of high order with respect to N.

On the other hand, the efficiency of multiphonon resonant Raman scattering that takes into account only uncorrelated electron–hole pair states as intermediate states does not contain any decreasing parameter. It is qualitatively clear that a negligibly small value of γ_d in the probability of the cascade process via electron–hole pairs protects the cross section from a rapid decrease with increasing N. The cross section $\sigma_N^{\rm EHP}$ is proportional to α^3 for $N\geqslant 4$. However, this mechanism cannot account for the strong outgoing resonance at $\omega_s=\omega_{\rm exc}$.

A combined scattering mechanism involving states of electron–hole pairs (the exciton continuum) and discrete energy states of Wannier–Mott excitons was recently proposed in Ref. 1 to explain the observation of both high-order phonon replicas and outgoing excitonic resonance.

The importance of taking into account the states of the

 1063-7761/96/090542-11$10.00

exciton continuum also follows from the theory of the monomolecular creation of discrete excitons from hot electron–hole pairs. In the monomolecular process a discrete exciton is created by a hot electron and a hot hole, which are created simultaneously in a photon absorption event and subsequently maintain their spatial correlation until the last step of the process, in which they bind to form an exciton after cooling as a result of the emission of several LO phonons. The initial steps in the direct creation of a hot electron–hole pair followed by the emission of $N-1$ phonons are the same as in multiphonon resonant Raman scattering involving free electron–hole pairs.

We have shown[2] that the strong outgoing excitonic resonance in multiphonon resonant Raman scattering in polar semiconductors occurs because the high-energy intermediate electron states are exciton states of the continuous spectrum (states of the exciton continuum); the electron–hole pairs bind to form excitons (exciton states of the discrete spectrum) only in the last step of the light scattering process. The electron–hole pairs cooled as a result of the emission of LO phonons bind to form excitons, whose energy is no longer sufficient for decay into electron–hole pairs with the emission of LO phonons.

The high probability of exciton decay (transitions to the continuum) strongly inhibits attributing the experimentally observed outgoing excitonic resonance to multiphonon resonant Raman scattering involving only bound excitonic intermediate states. Below, we analyze the influence of a strong magnetic field on the monomolecular mechanism for creating a "cold exciton" from pairs created by light and on outgoing excitonic resonance. Although they lose energy, electron–hole pairs maintain their spatial correlation when they interact with LO phonons.

2. WAVE FUNCTION OF AN EXCITON IN A MAGNETIC FIELD

The main contribution to Nth-order multiphonon resonant Raman scattering comes from processes represented in Figs. 1(a) and 1(b) with one or two excitonic intermediate states in the last step of the process. Only these contributions correspond to cascade transitions, in which the bound exciton states cannot undergo transitions to continuum states with the emission of LO phonons. It will be assumed below that the hole effective mass is considerably greater than the electron effective mass, i.e., $m_h \gg m_e$, and that the hole energy is consequently small, so that all phonons emitted by electron–hole pairs before they bind to form an exciton are emitted by the electron.

We consider only the ground state ($n=0$) of an exciton in a strong magnetic field. The gauge of the vector potential of the external constant uniform magnetic field is chosen in the form $\mathbf{A}=\mathbf{A}(0,\ xH,\ 0)$. The wave function of an exciton, which depends on its exciton wave vector $\mathbf{K}$, has the form[2,3]

$$\Psi^{\mathrm{exc}}_{\mathbf{K}_\perp K_z}=\Psi_{\perp\mathbf{K}_\perp}\Psi_{\parallel K_z},$$

$$\Psi_{\perp\mathbf{K}_\perp}=\frac{1}{a_H\sqrt{2\pi L_x L_y}}\exp\left\{i\left[\left(K_x-\frac{y}{a_H^2}\right)R_x+K_yR_y+\Phi(\mathbf{r}_\perp,-\mathbf{K}_\perp)+C(K_x,K_y)\right]\right\}K_{00}\left(\frac{\mathbf{r}_\perp-\mathbf{r}_\perp(\mathbf{K}_\perp)}{a_H}\right),$$

$$\Phi(\mathbf{r}_\perp,-\mathbf{K}_\perp)=\frac{m_e-m_h}{2M}\left(\frac{xy}{a_H^2}-K_xx-K_yy\right),$$

$$C(K_x,K_y)=\frac{m_e-m_h}{2M}a_h^2K_xK_y,$$

$$K_{nm}(\mathbf{p})=\left(\frac{\min(n!,m!)}{\max(n!,m!)}\right)^{1/2}i^{|n-m|}\exp\left(-\frac{p^2}{4}\right)\times\left(\frac{p}{\sqrt{2}}\right)^{|n-m|}\exp\left[i\left(\phi-\frac{\pi}{2}\right)(n-m)\right]L^{|n-m|}_{\min(n,m)}\left(\frac{p^2}{2}\right), \tag{1}$$

where $a_H=\sqrt{c\hbar/eH}$, $L_m^n(x)$ is an associated Laguerre polynomial, and $\mathbf{r}_\perp(\mathbf{K}_\perp)=(a_H^2/H)(\mathbf{HK}_\perp)$.

The function $\Psi_{\perp\mathbf{K}_\perp}$ can be written as the sum

$$\Psi_{\perp\mathbf{K}_\perp}=\sqrt{\frac{2\pi a_H^2}{L_xL_y}}\frac{1}{L_y}\sum_{k_{1y},k_{2y}}\delta_{K_y,k_{1y}+k_{2y}}\times\exp(-ia_H^2K_xk_y)\times\exp[i(k_{1y}y_1+k_{2y}y_2)]\Phi_0(x_1+a_H^2k_{1y})\Phi_0(x_2-a_H^2k_{2y}), \tag{2}$$

where

$$\Phi_0(x)=\sqrt{\frac{1}{\sqrt{\pi}a_H}}\exp\left(-\frac{x^2}{2a_H^2}\right),$$

$$k_y=\frac{k_{1y}m_h-k_{2y}m_e}{M}, \tag{3}$$

and k_1 (k_2) is the wave vector of the electron (hole). It can be shown that the right-hand sides of the expressions for $\Psi_{\perp\mathbf{K}_\perp}$ in (1) and (2) are exactly equal to one another.

The longitudinal part of the exciton wave function from (1) can be written in the form

$$\Psi_{\parallel K_z}=\frac{1}{\zeta\sqrt{a_\parallel L_z}}\exp(iK_zR_z)\xi\frac{z}{a_\parallel}, \tag{4}$$

where $\xi(t)$ is a certain function for which $\xi(t=0)=1$. The constant ζ is given by the normalization condition

$$\zeta^2=\int_{-\infty}^{\infty}dt\ \xi^2(t).$$

The coordinates of the electron (hole) are denoted by x_1,y_1 (x_2,y_2), and the coordinates of the total and relative motion of the electron–hole pair are:

$$\mathbf{R}=(m_e\mathbf{r}_1+m_h\mathbf{r}_2)/M,\quad \mathbf{r}=\mathbf{r}_e-\mathbf{r}_h,\quad M=m_e+m_h.$$

3. BASIC ELEMENTS OF THE DIAGRAM TECHNIQUE

The exciton wave function defined in Ref. 3 transforms into the function (1) if the Landau gauge, rather than a symmetric gauge of the vector potential, is chosen. The functions (2) and (4) were used in Ref. 2, the unimportant phase factor $iC(K_x,K_y)$ being omitted, the function $\xi(t)$ being taken in the form $\xi(t)=\exp(-t^2/4)$, and ζ being equal to $(2\pi)^{-1/4}$. We use the exciton wave function (1) to devise a diagram technique. We formulate the rules of the diagram technique[1)] for calculating the scattering tensor $S_{\alpha\gamma\beta\lambda}$ in the presence of a strong magnetic field. The intermediate states of the system are taken into account in the form of Wannier–Mott excitons in the internal ground state.

1. A contour consists of two segments of a single straight line. The vertices of the interaction with light labeled α and γ, are located on the left-hand segment, and the vertices labeled β and γ are located on the right-hand segment.

2. Wave vectors κ_l (κ_s) are associated with the photon lines, i.e., the dotted lines. We set $\kappa_l\simeq\kappa_s\simeq 0$.

3. Electron (solid) lines are located above the contour line, and Hole lines are located below it. The indices n, k_y, and k_z are associated with them.

4. Solid exciton lines lie on the contour line. The wave vector $\mathbf{K}$ is associated with the exciton lines. Phonon lines are dashed. The wave vector $\mathbf{q}$ is associated with them.

We write out the factors corresponding to the vertices on the left-hand segment of the contour C_1.

5. An unfilled point (vertex) into which a photon line enters and from which an electron line and a hole line emerge corresponds to a factor

$$J_\gamma=\frac{e}{m_0}p_{cv,\gamma},$$

where e is the absolute value of the electron charge, m_0 is the free-electron mass, and $\mathbf{p}_{cv}$ is an interband matrix element of the momentum operator. The indices n of the electron and hole lines should coincide.

An unfilled point (vertex) into which a $\mathbf{K}=0$ exciton line enters and from which a photon line emerges is associated with a factor

$$J_{\alpha,\mathrm{exc}}=\frac{e}{m_0}p^*_{cv,\alpha}\frac{\sqrt{V_0}}{\sqrt{2\pi}\zeta a_H\sqrt{a_\parallel}}.$$

6. Filled points (vertices) denote interactions of the electronic system with LO phonons.

A vertex into which an electron (hole) line with indices n, k_y, and k_z enters and from which an electron (hole) line with indices n', k'_y and k'_z and $\mathbf{q}$ phonon line emerges is associated with a factor

$$\left(\mp\frac{i}{\hbar}\right)C^*_{\mathbf{q}}\exp\left[\mp ia_H^2q_x\left(k_y-\frac{q_y}{2}\right)\right]K_{nn'}(\pm a_Hq_y,-a_Hq_x),$$

where the upper (lower) signs correspond to the electron (hole),

$$C_{\mathbf{q}}=-i\hbar\omega_{\mathrm{LO}}\sqrt{\frac{4\pi\alpha l^3}{V_0}}\frac{1}{ql},\qquad l=\sqrt{\frac{\hbar}{2m_e\omega_{\mathrm{LO}}}},$$

$$\alpha=\frac{e^2}{2\hbar\omega_{\mathrm{LO}}l}\left(\frac{1}{\epsilon_\infty}-\frac{1}{\epsilon_0}\right),\tag{5}$$

ϵ_0 (ϵ_∞) is the static (high-frequency) dielectric constant, and $K_{nn'}(\mathbf{p})=K_{\eta\eta'}(p_x,p_y)$ is defined by (1).

7. A vertex into which a $\mathbf{K}$ exciton line enters and from which a $\mathbf{q}$ phonon line and a $\mathbf{K}'=\mathbf{K}-\mathbf{q}$ exciton line emerge corresponds to a factor $-(i/\hbar)C_{\mathrm{exc}}$, where

$$C_{\mathrm{exc}}=C_{\mathrm{exc},e}+C_{\mathrm{exc},h},$$

$$C_{\mathrm{exc},e(h)}=\pm\zeta^{-2}C^*_{\mathbf{q}}\exp[i(\varphi\pm\varphi_1)]\times\exp(-a_H^2q_\perp^2/4)\,\eta(a_\parallel q_z m_{h(e)}/M),\tag{6}$$

the upper (lower) signs correspond to e (h),

$$\varphi=\frac{m_l-m_h}{2M}a_H^2(K_xK_y-K'_xK'_y),$$

$$\varphi_1=\frac{a_H^2}{2}(q_xK_y-K_xq_y),\qquad \eta(\alpha)=\int_{-\infty}^{\infty}dt\,e^{i\alpha t}\xi^2(t).$$

The vertex into which the electron line labeled n_1,k_{1y},k_{1z} and the hole line labeled n_2,k_{2y},k_{2x} enter and from which the $\mathbf{K}$ exciton line and the $\mathbf{q}$ phonon line emerge corresponds to a factor $-(i/\hbar)C_{\mathrm{EHP-exc}}$, where

$$C_{\mathrm{EHP-exc}}=C_{\mathrm{EHP-exc},e}+C_{\mathrm{EHP-exc},h}.$$

Here

$$C_{\mathrm{EHP-exc},e}=\frac{\sqrt{2}\pi}{\zeta}\frac{a_H\sqrt{a_\parallel}}{\sqrt{V_0}}C^*_{\mathbf{q}}\exp[i(\psi+\psi_1)]\exp\left[iq_xa_H^2\left(k_{1y}-\frac{q_y}{2}\right)\right]\delta_{n_2,0}\times K_{n_1,0}(a_Hq_y,-a_Hq_x)\,\theta\left(\left[k_z-\frac{q_zm_h}{M}\right]a_\parallel\right),$$

$$C_{\mathrm{EHP-exc},h}=-\frac{\sqrt{2}\pi}{\zeta}\frac{a_H\sqrt{a_\parallel}}{\sqrt{V_0}}C^*_{\mathbf{q}}\exp[i(\psi-\psi_1)]\exp\times\left[-iq_xa_H^2\left(k_{2y}-\frac{q_y}{2}\right)\right]\delta_{n_1,0}K_{n_1,0}(-a_Hq_y,-a_Hq_x)\,\theta\left(\left[k_z+\frac{q_zm_e}{M}\right]a_\parallel\right),$$

where

$$\psi=a_H^2\left(K_xk_y+K_xq_y\frac{m_e-m_h}{2M}\right),$$

$$\psi_1=-\frac{a_H^2}{2}K_xq_y,$$

$$k_y=\frac{m_hk_{1y}-m_ek_{2y}}{M},\qquad k_z=\frac{m_hk_{1z}-m_ek_{2z}}{M}$$

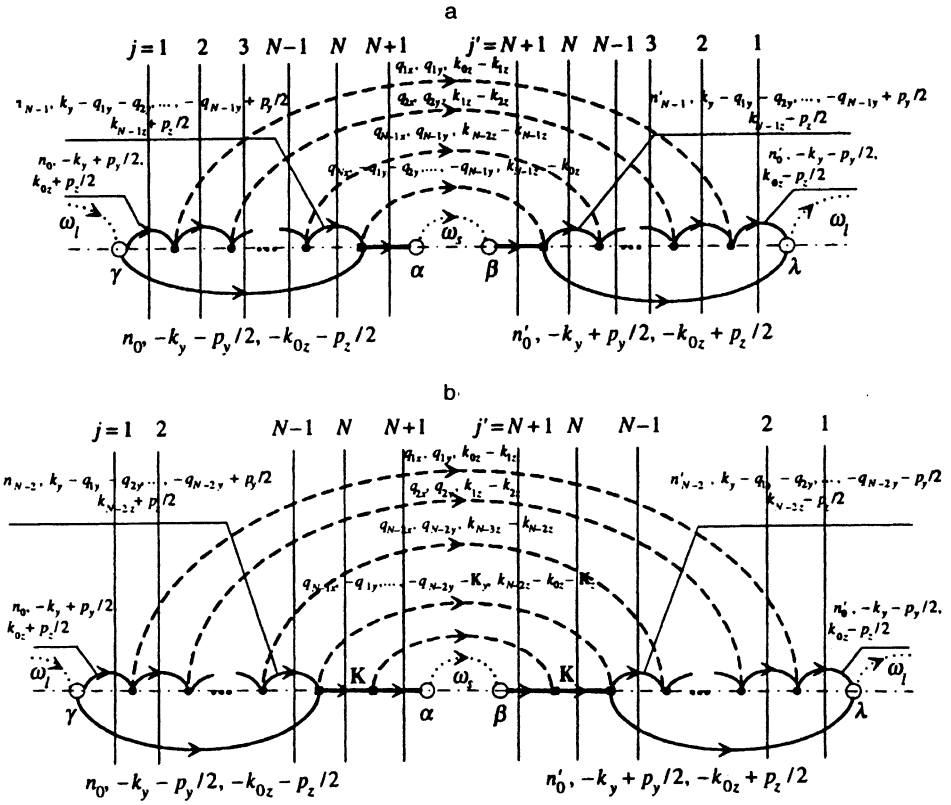

FIG. 1. Two diagrams with one (a) and two (b) discrete excitonic intermediate states making the dominant contribution to the multiphonon resonant Raman scattering in the region of outgoing resonance. The filled points (vertices) correspond to an electron–phonon interaction, and the unfilled points (vertices) correspond to transitions between discrete states and transitions between discrete and continuum states.

are the components of the wave vector for the relative motion of the electron and the hole, and

$$\theta(\alpha)=\int_{-\infty}^{\infty} dt\, e^{i\alpha t}\xi(t).$$

8. Vertices on the right-hand segment of the contour that are mirror images of vertices on the left-hand segment correspond to complex-conjugate quantities.

When $\xi(t)=\exp(-|t|)$, we have

$$\zeta=1, \qquad \eta(\alpha)=\frac{1}{1+\alpha^2/4}, \qquad \theta(\alpha)=\frac{2}{1+\alpha^2}.$$

9. Vertical sections labeled j on the left-hand part of the contour (between the unfilled points) are associated with a factor

$$(\omega_l-E_j/\hbar+i\gamma_j/2)^{-1},$$

where E_j is the sum of the energies of all the lines intersecting these sections and γ_j is the sum of the reciprocal lifetimes.

On the right-hand side of the contour the section labeled j' corresponds to a factor

$$(\omega_l-E_{j'}/\hbar-i\gamma_{j'}/2)^{-1}.$$

The energy of an electron line is

$$\left(n+\frac{1}{2}\right)\hbar\omega_{eH}+\frac{\hbar^2k_z^2}{2m_e},$$

and the energy of a hole line is

$$\hbar\omega_g+\left(n+\frac{1}{2}\right)\hbar\omega_{hH}+\frac{\hbar^2k_z^2}{2m_h},$$

where $E_g=\hbar\omega_g$ is the band gap of the semiconductor in the absence of a magnetic field,

$$\omega_{eH}=\frac{eH}{m_ec}, \qquad \omega_{hH}=\frac{eH}{m_hc}.$$

Each exciton line has energy $E_{\rm exc}(K_\perp,|K_z|)$, which is measured from the ground-state energy of the crystal. The damping of an electron in the presence of a strong magnetic field is denoted by $\gamma_e(n,|k_z|)$, the damping of a hole is denoted by $\gamma_h(n,|k_z|)$, and the damping of an exciton is denoted by $\gamma_{\rm exc}(K_\perp,|K_z|)$. The damping of phonons is neglected.

10. The entire result is multiplied by

$$\frac{1}{V_0\hbar^2\omega_s^2\omega_l^2}\,\delta(\omega_l-\omega_s-N\omega_{\rm LO}).$$

4. BASIC DIAGRAMS

Figures 1(a) and 1(b) display the diagrams which, under the condition $m_h\gg m_e$, make the main contribution to the scattering cross sections near the resonance $\hbar\omega_s=E_{1H}=\hbar\omega_{1H}$, where $E_{1H}=E_{\rm exc}(K_\perp=0,\ K_z=0)$. The diagram in Fig. 1(a) describes a process in which all intermediate states except the last are free electron–hole pair states, and only the last $(N+1)$th intermediate state corre-

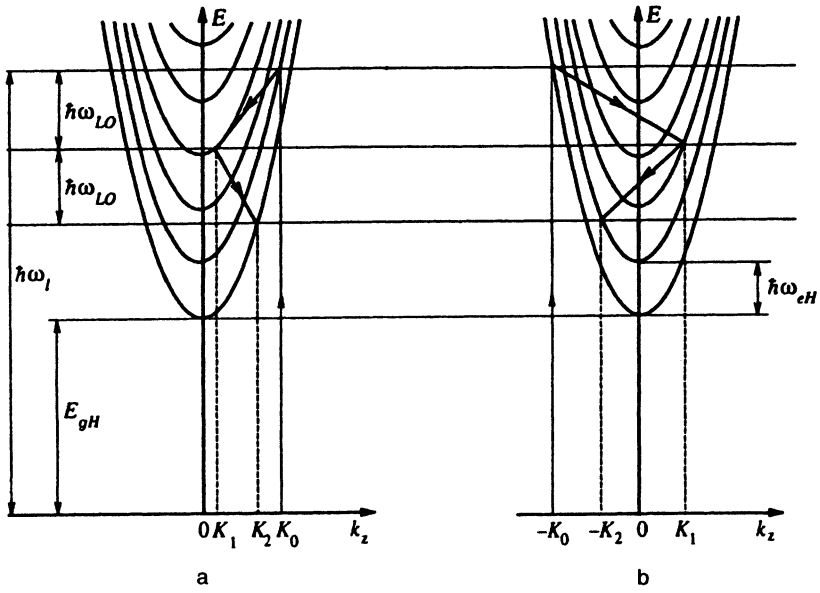

FIG. 2. Raman-scattering frequency intervals.

sponds to an exciton. Figure 1b displays a diagram in which the last two intermediate states are exciton states. The numbers of these states are N and $N+1$.

The following approximations are used to calculate the contributions of the diagrams in Fig. 1. Assuming that $m_h \gg m_e$, we set $m_h^{-1}=0$ and $\gamma_h=0$ in the energy denominators. We assume that $p_z \sim \lambda^{-1}$, where λ is the electron mean free path, which is restricted by the possibility of the emission of an LO phonon. Therefore, we assume that

$$p_z \ll K_j, \qquad p_z \ll a_\parallel,$$

where K_j is the resonant value of the projection of the electron wave vector onto the z axis (see below). We consider only the contributions of diagrams for which

$$n_0'=n_0, \qquad n_1'=n_1, \ldots, n_{N-1}'=n_{N-1}.$$

We calculate the tensor according to the same scheme as in Ref. 5. The scattering efficiency is expressed in terms of the light scattering tensor in the following manner:

$$\frac{d^2S}{do\,d\omega_s}=\frac{\omega_s^3\omega_l}{c^4}\frac{n_s}{n_l}e_{s\alpha}^*e_{s\beta}e_{l\gamma}\,e_{l\lambda}^*S_{\alpha\gamma\beta\lambda}(\omega_l,\omega_s,\kappa_l,\kappa_s), \tag{7}$$

where $S_{\alpha\gamma\beta\lambda}$ is the fourth-rank light scattering tensor, c is the speed of light in vacuum, n_l (n_s), $\mathbf{e}_l$ ($\mathbf{e}_s$), and κ_l (κ_s) are the refractive index, the polarization vector, and the wave vector of the incident (scattered) light, respectively. For the contributions of the diagrams in Fig. 1 we obtain the result

$$\frac{d^2S_{Na(b)}}{do\,d\omega_s}=\sigma_0\frac{\omega_s n_s}{\omega_l n_l}\frac{|\mathbf{e}_l\mathbf{p}_{cv}|^2|\mathbf{e}_s\mathbf{p}_{cv}|^2}{m_0^2\hbar^2}\delta(\omega_l-\omega_s-N\omega_{\mathrm{LO}})$$
$$\times[(\omega_s-\omega_{1H})^2$$
$$+(\gamma_{\mathrm{exc}H}(0)/2)^2]^{-1}(\pi a_H^2)^{-1}L_{Na(b)}^{-1}, \tag{8}$$

where $\sigma_0=(e^2/m_0c^2)^2$, $\gamma_{\mathrm{exc}H}(0)$ is the lifetime of an exciton in the ground state. The quantity $L_{Na(b)}^{-1}$ has the dimensions of reciprocal length and various values for the contributions of the diagrams in Figs. 1(a) and 1(b).

For the diagram in Fig. 1(a) we have

$$L_{Na}^{-1}=\sum_\beta \frac{Z_{N\beta}}{\Lambda_{N\beta}}\Xi_{n_0,n_{N-1}}, \tag{9}$$

where the subscript β labels the "trajectory" that the electron follows among the Landau bands, while successively emitting $N-1$ phonons. Examples of such "trajectories" are shown in Fig. 2. The subscript β consists of the set of indices $n_0, n_1, \ldots, n_{N-1}$ of the Landau bands, and the set of indices $i, i_2, \ldots, i_{N-1}$, each of which can take two values: 0 and 1. The subscript 0 denotes the absence of turning of the electron as it moves along the z axis and emits an LO phonon, and the subscript 1 indicates turning of the electron. For example, in Fig. 2(a) $n_0=1$, $n_1=3$, $n_2=0$, $i_1=0$, $i_2=0$; in Fig. 2(b) $n_0=0$, $n_1=3$, $n_2=1$, $i_1=1$, $i_2=1$. The following notation is used:

$$Z_{N\beta}=D_{N\beta}/Y_{N\beta},$$

$$D_{N\beta}=(K_0K_1\ldots K_{N-1})^{-1}\int_0^\infty dx_1\int_0^\infty dx_2\ldots\int_0^\infty dx_{N-1}$$
$$\times B_{n_0n_1}(x_1)\chi^{i_1}(K_0,K_1,x_1)B_{n_1n_2}$$
$$\times(x_2)\chi^{i_2}(K_1,K_2,x_2)\ldots$$
$$\times\ldots B_{n_{N-2}n_{N-1}}(x_{N-1})\chi^{i_{N-1}}(K_{N-2},K_{N-1},x_{N-1})$$
$$\times\overline{B_{n_{N-1}n_0}(x_N)\chi^{i_N}(K_{N-1},K_0,x_N)}, \tag{10}$$

$$K_j=\sqrt{(2m_e/\hbar)(\omega_l-\omega_{gH}-n_j\omega_eH-j\omega_{\mathrm{LO}})} \tag{11}$$

are the values of the projection k_z of the electron wave vector after the emission of j LO phonons according to the energy conservation law (see Fig. 2), $E_{gH}=E_g+\hbar eH/2\mu c$ is the band gap of the semiconductor in a strong magnetic field, $\mu=m_em_h/M$,

$$B_{nn'}(x)=\frac{\min(n!,n'!)}{\max(n!,n'!)}e^{-x}x^{|n-n'|}[L^{|n-n'|}_{\min(n,n')}(x)]^2, \quad (12)$$

and

$$\chi^i(K,K',x)=[x+(a_H^2/2)(K\mp K')^2]^{-1}, \quad (13)$$

the upper minus sign corresponding to $i=0$ (no turning) and the lower plus sign corresponding to $i=1$ (turning). The superscript i_n indicates whether the direction of k_z after the emission of $N-1$ phonons coincides with its original direction. It is easily seen that $i_N=0$, if s is an even number, and $i_N=1$, if s is odd, where

$$s=\sum_{n=1}^{N-1} i_N.$$

The overline on the right-hand side of (10) denotes averaging over the angles that specify the directions of the vectors $\mathbf{q}_{1\perp}$, $\mathbf{q}_{2\perp}, \ldots, \mathbf{q}_{N-1\perp}$ in the xy plane, if

$$x_1=\frac{a_H^2q_{1\perp}^2}{2}, \quad x_2=\frac{a_H^2q_{2\perp}^2}{2}, \ldots, x_{N-1}=\frac{a_H^2q_{N-1\perp}^2}{2}, \quad x_N=\frac{a_H^2q_{N\perp}^2}{2}, \quad \mathbf{q}_{N\perp}=-\mathbf{q}_{1\perp}-\mathbf{q}_{2\perp}-\ldots-\mathbf{q}_{N-1\perp}. \quad (14)$$

The following notation is also used:

$$Y_{N\beta}=\gamma_0\gamma_1\ldots\gamma_{N-1}\left(\frac{2l}{\alpha\omega_{\mathrm{LO}}}\right)^N, \quad \gamma_j=\gamma_e(n_j,K_j). \quad (15)$$

If the reciprocal lifetime $\gamma_j=\gamma_e(n_j,K_j)$ of the electron is defined by the emission probability of an LO phonon, according to Ref. 5 we have

$$\gamma_e(n,|k_z|)=\alpha\omega_{\mathrm{LO}}\sum_{n'}\frac{1}{2l|k_z'|}\int_0^\infty dxB_{nn'}(x)\times[\chi^0(|k_z|,|k_z'|,x)+\chi^1(|k_z|,|k_z'|,x)], \quad (16)$$

$$k_z'=\sqrt{k_z^2+(2m_e/\hbar)[\omega_{eH}(n-n')-\omega_{\mathrm{LO}}}.$$

On the right-hand side of (16) only the indices for which k_z' is real are included in the sum over n'. If all the parameters $\gamma_0,\gamma_1,\ldots,\gamma_{N-1}$ are determined by the real emission of LO phonons, then, substituting (16) into (15), we obtain the expression for $Y_{N\beta}$ presented in Ref. 5 (Eq. (134)), i.e.,

$$Y_{N\beta}=\sum_{n_0'}\left\{\frac{1}{K_0'}\int_0^\infty dxB_{n_0n_0'}(x)[\chi^0(K_0,K_0',x)+\chi^1(K_0,K_0',x)]\right\}\sum_{n_1'}\left\{\frac{1}{K_1'}\int_0^\infty dxB_{n_1n_1'}(x)\times[\chi^0(K_1,K_1',x)+\chi^1(K_1,K_1',x)]\right\}\ldots\sum_{n_{N-1}'}\times\left\{\frac{1}{K_{N-1}'}\int_0^\infty dxB_{n_{N-1}n_{N-1}'}(x)[\chi^0(K_{N-1},K_{N-1}',x)+\chi^1(K_{N-1},K_{N-1}',x)]\right\}. \quad (17)$$

However, near the resonance point $\hbar\omega_s=E_{1H}=\hbar\omega_{1H}$ the emission of an LO phonon by an electron that has already emitted $N-1$ phonons is impossible due to a lack of energy, and γ_{N-1} is determined by some other processes, so that we can set

$$\gamma_{N-1}=\Gamma_{N-1}, \quad \Gamma_{N-1}\ll\gamma_j, \quad j=0, \quad 1,\ldots,N-2. \quad (18)$$

We then obtain

$$Y_{N\beta}=Y_{N-1\beta}\frac{2l\Gamma_{N-1}}{\alpha\omega_{\mathrm{LO}}}, \quad (19)$$

where $Y_{N-1,\beta}$ is determined from (17). The quantity $\Lambda_{N\beta}$ (with dimensions of length) is defined as

$$\Lambda_{N\beta}=f_{N\beta}^{-1}(z=0), \quad f_{N\beta}(z)=f^{i_1i_2\ldots i_{N-1}}(z). \quad (20)$$

For example,

$$f^{010}(z)=\frac{1}{2}[f^{++--}(z)+f^{--++}(z)],$$

$$f^{++--}(z)=\frac{1}{\lambda_0\lambda_1\lambda_2\lambda_3}\int_{-\infty}^\infty dz_0\int_{-\infty}^\infty dz_1\int_{-\infty}^\infty dz_2\Upsilon^+\left(\frac{z_0}{\lambda_0}\right)\Upsilon^+\left(\frac{z_1-z_0}{\lambda_1}\right)\times\Upsilon^+\left(\frac{z_2-z_1}{\lambda_2}\right)\Upsilon^+\left(\frac{z-z_2}{\lambda_3}\right),$$

$$\lambda_j=\frac{\hbar K_j}{m_e\gamma_j}, \quad \gamma_j=\gamma_e(n_j,K_j), \quad (21)$$

$$\Upsilon^+(t)=\begin{cases}e^{-t}, & t>0,\\ 0, & t<0,\end{cases} \quad (22)$$

$$\Upsilon^-(t)=\begin{cases}0, & t>0,\\ e^t, & t<0.\end{cases}$$

In the p-representation, for example, we have

$$f^{++--}(z)=\frac{1}{2\pi}\int_{-\infty}^\infty dpe^{ipz}[(1+i\lambda_0p)(1+i\lambda_1p)(1-i\lambda_2p)(1-i\lambda_3p)]^{-1}. \quad (23)$$

Finally, we use the notation

$$\Xi_{n_0,n_{N-1}}=[\delta_{n_0,0}\theta^2(a_\parallel K_0)+\delta_{n_{N-1},0}\theta^2(a_\parallel K_{N-1})-2\delta_{n_0,0}\delta_{n_{N-1},0}\theta(a_\parallel K_0)\theta(a_\parallel K_{N-1})\zeta^{-4}. \quad (24)$$

5. CONTRIBUTION OF THE DIAGRAM IN FIG. 1b

Before presenting the result for the contribution of the diagram in Fig. 1(b) to the scattering efficiency, we interpret the notation $E_{\mathrm{exc}}(K_\perp,|K_z|)$ for the exciton energy in the internal ground state with the wave vector $\mathbf{K}$, since the diagram in Fig. 1(b) corresponds to the next-to-last intermediate state for which $\mathbf{K}\neq 0$. We write the exciton energy as

$$E_{\rm exc}(K_\perp,|K_z|)=E_{gH}+E(K_\perp)+\frac{\hbar^2K_z^2}{2M}. \tag{25}$$

Expressions for $E(K_\perp)$ in some limiting cases were presented in Ref. 3, but we shall not use them, and we merely note that $E(K_\perp=0)=-\Delta E_{1H}$ is the binding energy of the exciton in the ground state in a strong magnetic field, and $E_{1H}=E_{gH}-\Delta E_{1H}$.

Thus, for the contribution of the diagram in Fig. 1(b) we obtain the result (8), where

$$L_{Nb}^{-1}=\alpha\omega_{\rm LO}\frac{M}{m_e}\int_0^{x_{\max}} \times dx e^{-x}\frac{[\eta(a_\parallel K_{z0}m_h/M)-\eta(a_\parallel K_{z0}m_e/M)]^2}{\zeta^4(x+a_H^2K_{z0}^2/2)^2 lK_{z0}\gamma_{\rm exc}(x,K_{z0})} \times\sum_\beta\frac{G_{N-1\beta}(x,K_{z0})}{\Lambda_{N-1\beta}}. \tag{26}$$

Here we have introduced the integration variable x and the following notation:

$$x=a_H^2K_\perp^2/2,\qquad x_{\max}=a_H^2K_{\perp\max}^2/2,$$

$$K_{z0}=\sqrt{\frac{2M}{\hbar}\left[\omega_l-\omega_{gH}-\frac{E(x)}{\hbar}-(N-1)\omega_{\rm LO}\right]},$$

which is the absolute value of the projection of the exciton wave vector in the real intermediate (next-to-last) state of the crystal onto the z, and $K_{\perp\max}$, which is the maximum value of $K_\perp$ permitted by the energy conservation law, i.e., the maximum value at which K_{z0} is real. As $K_\perp$ varies from zero to infinity, $E(x)$ varies from $-\Delta E_{1H}$ to zero;[2] therefore, over the range

$$\omega_l>\omega_{gH}+(N-1)\omega_{\rm LO} \tag{27}$$

we have $x_{\max}\to\infty$, and over the range

$$E_{1H}/\hbar+(N-1)\omega_{\rm LO}<\omega_l<\omega_{gH}+(N-1)\omega_{\rm LO}$$

$K_{\perp\max}$ and $x_{\max}$ are specified by

$$\hbar\omega_l-E_{gH}-(N-1)\hbar\omega_{\rm LO}-E(K_{\perp\max}). \tag{28}$$

We also introduce the notation

$$G_{N-1\beta}(x,K_{z0})=\frac{R_{N-1\beta}(K_\perp,K_{z0})}{Y_{N-1\beta}}, \tag{29}$$

where β denotes the set of indices $n_0, n_1\ldots, n_{N-2}, i_1,i_2\ldots, i_{N-2}$,

$$R_{N-1,\beta}(K_\perp,K_{z0})=\frac{1}{K_0K_1\ldots K_{N-2}}\int_0^\infty dx_1 \times\int_0^\infty dx_2\ldots\int_0^\infty dx_{N-2}B_{n_0n_1}(x_1)\chi^{i_1} \times(K_0,K_1,x_1)B_{n_1n_2}(x_2)\chi^{i_2}(K_1,K_2,x_2) \ldots B_{n_{N-1}n_{N-1}}(x_{N-2})\chi^{i_{N-2}} \times(K_{N-3},K_{N-2},x_{N-2}) \times\overline{B_{n_{N-2}n_0}(x_{N-1})P_\beta(K_\perp,K_{z0})}, \tag{30}$$

$$P_\beta(K_\perp,K_{z0})=\frac{1}{2}[\Upsilon_\beta(K_\perp,K_{z0})+\Upsilon_\beta(K_\perp,-K_{z0})], \tag{31}$$

$$\Upsilon_\beta(K_\perp,K_{z0})=\zeta^{-4}\{x_{N-1}+(a_H^2/2)[(-1)^pK_{N-2}-K_0 -K_{z0}]^2\}^{-1}\left\{\delta_{n_0,0}\theta^2\left(a_\parallel\left[K_0+\frac{m_hK_{z0}}{M}\right]\right) +\delta_{n_{N-2},0}\theta^2\left(a_\parallel\left[(-1)^pK_{N-2}-\frac{m_eK_{z0}}{M}\right]\right) -2\delta_{n_0,0}\delta_{n_{N-2},0}\theta\left(a_\parallel\left[K_0+\frac{m_hK_{z0}}{M}\right]\right)\theta\left(a_\parallel\left[(-1)^pK_{N-2}-\frac{m_eK_{z0}}{M}\right]\right)\cos[a_H^2(\mathbf{q}_{N-1}\mathbf{K}_\perp)]\right\}. \tag{32}$$

In (30) we introduced the integration variables

$$x_1=\frac{a_H^2q_{1\perp}^2}{2},\qquad x_2=\frac{a_H^2q_{2\perp}^2}{2},\ldots,x_{N-2} =\frac{a_H^2q_{N-2\perp}^2}{2},\qquad x_{N-1}=\frac{a_H^2q_{N-1\perp}^2}{2},$$

$$\mathbf{q}_{N-1\perp}=-\mathbf{q}_{1\perp}-\mathbf{q}_{2\perp}-\ldots-\mathbf{q}_{N-1\perp}-\mathbf{K}_\perp. \tag{33}$$

The overline on the right-hand side of (30) denotes averaging over the angles that specify the direction of the vectors $\mathbf{q}_{1\perp}$, $\mathbf{q}_{2\perp}$, $\ldots$, $\mathbf{q}_{N-2\perp}$, $\mathbf{K}_\perp$ in the xy plane. The exponent p on the right-hand side of (32) is

$$p=\sum_{n=1}^{N-2}i_n.$$

Finally, $\gamma_{\rm exc}(x,K_{z0})=\gamma_{\rm exc}(K_\perp,K_{z0})$, where $x=a_H^2K_\perp^2/2$.

6. APPLICABILITY OF THE THEORY

Let us first determine the permissible values of the frequency ω_l. We infer that $\Delta E_H<\hbar\omega_{\rm LO}$. For a given scattering order N we consider four ranges of ω_l, which we define as

$$\begin{aligned}&a)\ \omega_{1H}+(N-1)\omega_{\rm LO}<\omega_l<\omega_{gH}+(N-1)\omega_{\rm LO},\\ &b)\ \omega_{gH}+(N-1)\omega_{\rm LO}<\omega_l<\omega_{1H}+N\omega_{\rm LO},\\ &c)\ \omega_{1H}+N\omega_{\rm LO}<\omega_l<\omega_{gH}+N\omega_{\rm LO},\\ &d)\ \omega_l>\omega_{gH}+N\omega_{\rm LO}.\end{aligned} \tag{34}$$

The widths of bands a and c are $\Delta E_H/\hbar$, and the width of band b is $\omega_{\rm LO}-\Delta E_H/\hbar$. The excitonic resonance point lies on the boundary between ranges b and c. Let us examine the applicability of (8) and (9) to the contribution of the diagram in Fig. 1(a). The expressions are applicable if K_{N-1} is real when $n_{N-1}=0$ (see the definition (11)), i.e., in ranges b, c, and d.

When $n_N=0$, K_N is imaginary in ranges b and c and real in range d. This means that the value of γ_{N-1} is specified by

Eq. (18), and Eq. (19) is applicable in ranges b and c, particularly in the vicinity of the excitonic resonance. We shall show that the value of Γ_{N-1} does not influence the result obtained for the contribution of the diagram in Fig. 1(a) to the scattering efficiency. Let us consider the factor $(Y_{N\beta}\Lambda_{N\beta})^{-1}$ appearing on the right-hand side of (9). It can be shown that when $\gamma_{N-1}\to\Gamma_{N-1}$ the value of $\Lambda_{N\beta}$, which is defined in (20), is proportional to the mean free path

$$\mathcal{L}_{N-1}=\frac{\hbar K_{N-1}}{m_e\Gamma_{N-1}},\quad \text{if } \mathcal{L}_{N-1}\gg\lambda_j,\quad j=0,1,\ldots,N-2, \tag{35}$$

i.e.,

$$\Lambda_{N\beta}^{-1}=\mathcal{L}_{N-1}^{-1}P_{N\beta}, \tag{36}$$

where $P_{N\beta}$ is a dimensionless quantity that depends on $\lambda_0,\lambda_1,\ldots,\lambda_{N-2}$. For example, for $N=2$ we have[2]

$$(\Lambda_2^0)^{-1}=f^0(z=0)=0,$$

$$(\Lambda_2^1)^{-1}=f^1(z=0)=(\lambda_0+\lambda_1)^{-1};$$

therefore,

$$P_2^0=0,\qquad P_2^1=1.$$

For $N=3$ we have

$$(\Lambda_3^{00})^{-1}=f^{00}(z=0)=0,\qquad (\Lambda_3^{10})^{-1}=f^{10}(z=0)$$

$$=\frac{\lambda_0}{(\lambda_0+\lambda_1)(\lambda_0+\lambda_2)},\qquad (\Lambda_3^{11})^{-1}=f^{11}(z=0)$$

$$=\frac{\lambda_1}{(\lambda_1+\lambda_0)(\lambda_1+\lambda_2)},\qquad (\Lambda_3^{01})^{-1}=f^{01}(z=0)$$

$$=\frac{\lambda_2}{(\lambda_2+\lambda_0)(\lambda_2+\lambda_1)}.$$

Assuming that $\lambda_2\to\mathcal{L}_2$, we obtain

$$P_3^{00}=0,\qquad P_3^{10}=\frac{\lambda_0}{\lambda_0+\lambda_1},\qquad P_3^{01}=1,$$

$$P_3^{11}=\frac{\lambda_1}{\lambda_0+\lambda_1}.$$

Using (19), (35), and (36), we obtain

$$(Y_{N\beta}\Lambda_{N\beta})^{-1}=(Y_{N-1\beta})^{-1}\frac{\alpha\omega_{\mathrm{LO}}m_e}{2l\hbar K_{n-1}}P_{N\beta}. \tag{37}$$

Thus, Γ_{N-1} drops out of the final result and does not influence its order of magnitude, Q.E.D.

Let us next consider the limits of applicability of Eqs. (8) and (26) to the contribution of the diagram in Fig. 1(b) to the scattering efficiency. These equations are applicable if K_{z0} is a real number, i.e., in all four ranges a, b, c, and d. In ranges b, c, and d, γ_{N-2} is determined by the real emission of LO phonons, but in range a

$$\Gamma_{N-2}\to\Gamma_{N-2},\qquad \Gamma_{N-2}\ll\gamma_j,\qquad j=0,1,\ldots,N-3,$$

and Γ_{N-2} does not appear in (26) for range a, as shown above.

The behavior of the reciprocal lifetime $\gamma_{\mathrm{exc}}(K_\perp,K_{z0})$, which appears in the denominator of (26), is very important for determining the contribution of the diagram in Fig. 1b. This reciprocal lifetime of the exciton corresponds to its energy,

$$E_{\mathrm{exc}}(K_\perp,K_{z0})=\hbar\omega_l-(N-1)\hbar\omega_{\mathrm{LO}}. \tag{38}$$

If

$$E_{\mathrm{exc}}(K_\perp,K_{z0})>E_{1H}+\hbar\omega_{\mathrm{LO}}, \tag{39}$$

$\gamma_{\mathrm{exc}}(K_\perp,K_{z0})$ is determined by the real probability of emission of an LO phonon by the exciton, and is proportional to α. In the opposite case, in which

$$E_{\mathrm{exc}}(K_\perp,K_{z0})<E_{1H}+\hbar\omega_{\mathrm{LO}}, \tag{40}$$

the real emission of an LO phonon by the exciton is impossible, and $\gamma_{\mathrm{exc}}(K_\perp,K_{z0})$ is determined by other, less likely processes, for example, by the interaction with acoustic phonons. Then

$$\gamma_{\mathrm{exc}}(K_\perp,K_{z0})\to\Gamma_{\mathrm{exc}}(K_\perp,K_{z0}),\quad \Gamma_{\mathrm{exc}}\ll\gamma_{\mathrm{exc}}. \tag{41}$$

The transition from (39) to (40) corresponds to the point of excitonic resonance. Below this point, where (40) holds, there is a sharp increase in the contribution of the diagram of Fig. 1(b) in comparison with the contribution of the diagram of Fig. 1a. Here additional diagrams containing acoustic phonon lines (see below) must be taken into account.

Let us determine the restrictions on the order N, which depend on the applicability of the polar approximation to the calculation of the integrals over k_{0z}, k_{1z}, ..., $k_{N-2,z}$ in the case of the diagram of Fig. 1(a) and over k_{0z}, k_{1z}, ..., $k_{N-2,z}$ in the case of Fig. 1(b). Similar calculations were described in Ref. 5. It is assumed *a priori* that values of p_z of order λ^{-1} are real and that $p_z\ll K_j$ and $p_z\ll a_\parallel^{-1}$. If the integrals over $p=p_z$ like (23) converge at large values of p, these assumptions are justified. When $p\to\infty$, the integrand is proportional to p^{-N} in the case of the diagram of Fig. 1(a) and to p^{-N+1} in the case of the diagram of Fig. 1(b). Therefore, Eq. (9) is applicable when $N\geq 2$, and Eq. (26) is applicable when $N\geq 3$. Finally, the following condition must hold for the results (9) and (26) to be valid:

$$\frac{\hbar K_j^2}{m_e}\gg\gamma_j.$$

Here $j=0,l,\ldots,N-1$ in the case of the diagram of Fig. 1(a), and $j=0,1,\ldots,N-2$ in the case of the diagram of Fig. 1(b).

7. RESONANT VALUES OF THE MAGNETIC FIELD

We confine ourselves to the condition $N\geq 3$, and then both equations, (9) and (26), are applicable. Examining these expressions, we see that both quantities increase as we approach $K_0=0$, which corresponds to the condition

$$(\omega_l)_{\max,m_h\to\infty}\simeq\omega_{gH}+n\omega_{eH}. \tag{42}$$

In the case of a finite-mass hole, instead of this relation we obtain the exact expression

$$(\omega_l(n))_{\max}=\omega_{gH}+\frac{eH}{\mu c}n. \tag{43}$$

The latter condition (43) means that light creates an electron and a hole near the bottoms of the Landau bands. A scattering efficiency maximum can be observed not only by varying ω_l at a fixed value of H, but also by varying the magnetic field strength at a fixed frequency ω_l. Solving Eq. (43), we find that maxima exist at values

$$H_{\max}(n)=\frac{\mu c}{e}\frac{\omega_l-\omega_g}{n+1/2}, \tag{44}$$

which do not depend on the scattering order N.

An additional resonance[2] appears only because of the contribution of the diagram of Fig. 1(b) for $N=3$ at values

$$(\omega_l')'_{\max,m_h\to\infty}\simeq\omega_{gH}+n\frac{eH}{m_ec}+\omega_{\mathrm{LO}} \tag{45}$$

due to the resonant increase in the quantity $(\Lambda_2^1)^{-1}=(\lambda_0+\lambda_1)^{-1}$ on the right-hand side of (26). In fact, the quantity

$$(\lambda_0+\lambda_1)^{-1}=\left(\frac{\hbar K_0}{m_e\gamma_0}+\frac{\hbar K_1}{m_e\gamma_1}\right)^{-1}$$

increases abruptly when $K_1\to 0$, since according to (16), γ_0 is singular when $K_1\to 0$ (see also Ref. 5). We also note that the contribution of the diagram of Fig. 1(b) vanishes at values

$$(\omega_l(n,N-2))_{\min,m_h\to\infty}=\omega_{gH}+\frac{eH}{m_ec}+(N-1)\omega_{\mathrm{LO}},$$

which depend on the scattering order.

8. SCATTERING BELOW THE EXCITONIC RESONANCE POINT

Above the excitonic resonance point, the contributions of the diagrams of Figs. 1(a) and 1(b) to the efficiency of multiphonon resonant Raman scattering are comparable. As we have already noted, when ω_l passes through the excitonic resonance in the downward direction, the contribution of the diagram of Fig. 1(b) increases sharply due to the increase in the lifetime of the exciton in the real intermediate state, and begins to dominate the contribution of the diagram of Fig. 1(a). The energy of the real exciton becomes too low to emit one LO phonon. Therefore, other processes, viz., absorption of LO phonons, interaction with acoustic phonons, etc., must be included in the theory.

Let us try to sketch a qualitative picture of the phenomenon with consideration of the distribution function of the real excitons with respect to the variables $K_\perp$ and $|K_z|$. We introduce the total Nth-order scattering efficiency

$$S_N=\int\int\frac{d^2S_N}{d\Omega d\omega_s}d\Omega d\omega_s, \tag{46}$$

which is distinguished from the quantity in (8) only by the absence of the factor $\delta(\omega_l-\omega_s-N\omega_{\mathrm{LO}})$ and the presence of the additional factor 4π (since the scattering is isotropic in our model). The expression for S_N can be written

$$S_N=\frac{l}{u_l}\sum_{\kappa_s}\bar{W}_s, \tag{47}$$

where $\bar{W}_s$ is the emission probability for a quantum of secondary radiation s per unit time normalized to one photon of exciting radiation.[6]

On the other hand, we have

$$\sum_{\kappa_s}W_{sN}=\sum_{K\perp,K_z}P_{\mathrm{exc},N-1}(K_\perp,|K_z|)\gamma_l(K_\perp,|K_z|), \tag{48}$$

where $P_{\mathrm{exc},N-1}(K_\perp,|K_z|)$ is the dimensionless distribution function of the real excitons[3)] with respect to the variables $K_\perp$ and $|K_z|$, and $\gamma_l(K_\perp,|K_z|)$ is the emission probability for a quantum of light together with one LO phonon by an exciton per unit time. We represent the probability $\gamma_l(K_\perp,|K_z|)$ in the form

$$\gamma_l(K_\perp,|K_z|)=\sum_{\kappa_s}w_s, \tag{49}$$

where

$$w_s=\frac{2\pi}{\hbar}\sum_j\left|\sum_a\frac{\langle f|U_s|a\rangle\langle a|H_{\mathrm{int}}|i\rangle}{E_i-E_a+i\hbar\gamma_a/2}\right|^2\delta(E_i-E_f) \tag{50}$$

is the emission probability for a quantum of light $\hbar\omega_s$ together with an LO phonon by an exciton per unit time, H_{int} is the Fröhlich interaction of the exciton with LO phonons, and U_s is the interaction of the exciton with light. The energies of the initial, final, and intermediate states are

$$E_i=E_{\mathrm{exc}}(K_\perp,|K_z|),\qquad E_f=\hbar\omega_s+\hbar\omega_{\mathrm{LO}},$$

$$E_a=E_{a\,EHP}+\hbar\omega_{\mathrm{LO}},$$

the intermediate electron–hole pair state including both exciton states belonging to the discrete spectrum and states of the continuous spectrum. Accordingly, we divide γ_l into two parts:

$$\gamma_l=\gamma_{l,\mathrm{disc}}+\gamma_{l,\mathrm{cont}}.$$

Excitonic resonance in light scattering is associated with the contribution of a transition via the exciton ground ($n=0$) state to $\gamma_{l,\mathrm{disc}}$. Therefore, we take into account and calculate only this contribution, which we denote by $\gamma_{l,\mathrm{disc},0}$. Performing calculations based on (47) and (48), we obtain

$$\gamma_{l,\mathrm{disc},0}(K_\perp,|K_z|)$$

$$=4\frac{n_s\omega_s}{\hbar c^3}\left(\frac{e}{m_0}\right)^2|\mathbf{e}_s\mathbf{p}_{cv}|^2\frac{\alpha\omega_{\mathrm{LO}}l}{K_\perp^2+K_z^2}\frac{1}{a_\parallel a_H^2\zeta^6}$$

$$\times\frac{\exp(-a_H^2K_\perp^2/2)[\eta(K_za_\parallel m_h/M)-\eta(K_za_\parallel m_e/M)]^2}{[\omega_{\mathrm{exc}}(K_\perp,|K_z|)-\omega_{lH}-\omega_{\mathrm{LO}}]^2+\gamma_{\mathrm{exc},H}^2(0)/4}. \tag{51}$$

For the range above excitonic resonance, i.e., at $\omega_l>N\omega_{\mathrm{LO}}+\omega_{lH}$, we have

$$P_{\text{exc},N-1}(K_\perp,|K_z|)=\frac{W_{\text{exc},N-1}(K_\perp,|K_z|)}{\gamma_{\text{exc}}(K_\perp,|K_z|)}, \quad (52)$$

where $W_{\text{exc},N-1}(K_\perp,|K_z|)$ is the number of excitons created per unit time in the volume V_0 together with the emission of $N-1$ LO phonons normalized to one photon of exciting radiation.

This quantity was calculated in Ref. 2 for $N-1=3$. Substituting the expression for $W_{\text{exc},N-1}(K_\perp,|K_z|)$ into (52) and then (51) and (52) into (47) and (48), we obtain the expression for the contribution of the diagram in Fig. 1b to the total Nth-order multiphonon resonant Raman scattering efficiency, which coincides with the contribution derived from Eqs. (8) and (26).

We note that above the excitonic resonance point, the distribution function of the excitons is nonzero over a very narrow energy range. In fact, the expression for $W_{\text{exc},N-1}(K_\perp,|K_z|)$ contains the δ function $\delta[\omega_l-(N-1)\omega_{\text{LO}}-E_{\text{exc}}(K_\perp,|K_z|)]$ (Ref. 2). However, the exciton distribution function becomes more diffuse at values of ω_l below the resonance point. We assume that the exciton distribution function is determined by the interaction with acoustic phonons. Then to calculate the light scattering efficiency the diagrams with external lines (joining the two segments of the contour) corresponding to acoustic phonons must be taken into account in the general case.

Emitting and absorbing acoustic phonons, the excitons slowly lose energy. The diffuseness should be far weaker at values of ω_l in range b than at frequencies in range a (see (34)), since real excitons with kinetic energies exceeding the exciton binding energy are created in range b. Since the probabilities of the exciton scattering and decay processes during the interaction with phonons are comparable, each exciton decays and "leaves the game" after several phonon absorption or emission events. Real excitons whose decay is hindered due to a lack of energy are created at values of ω_l in range a. In this case the exciton distribution function depends on the probability of the nonradiative annihilation of the latter, which, in turn, depends on the purity of the crystal. The exciton energy distribution function for $H=0$ was examined without considering decay, i.e., in range a, in Refs. 7–10.

The "erosion" of the exciton distribution function leads to considerable broadening of the multiphonon resonant Raman scattering peaks with respect to ω_s in range b and especially in range a and to a simultaneous increase in the total scattering intensity of a particular order in comparison with the contribution of the diagram of Fig. 1(b) given by (8) and (26). In fact, the diagrams that include external lines of acoustic phonons make positive contributions to the integrated scattering intensity.

Thus, the total intensity of the multiphonon resonant Raman scattering lines increases sharply upon passage through the excitonic resonance point $\omega_s=\omega_{1H}$ in the downward direction. Below this point the contribution of the diagram in Fig. 1(a) becomes relatively insignificant. The contributions of the processes not involving intermediate exciton states calculated in Ref. 5 are also insignificant when $\omega_s \leqslant \omega_{1H}$. Above the excitonic resonance point the contributions of the diagrams in Figs. 1(a) and 1(b) are comparable to one another, and at distances $\omega_s-\omega_{1H} \geqslant \omega_{\text{LO}}$ the contributions of diagrams without exciton states are comparable to them.

9. DISCUSSION

The main conclusion of this work is the sharp increase in the intensity of multiphonon resonant Raman scattering in the presence of a strong magnetic field. The values of the frequency ω_s of the scattered light considered range from just above the excitonic resonance point $\omega_s=\omega_{1H}/\hbar$ and extend below that point down to $\omega_s=\omega_{1H}-\omega_{\text{LO}}$. Above the excitonic resonance point there is an increase in the intensity by approximately α^{-2}-fold for any scattering order $N \geqslant 3$, since the cross section is proportional to α^3 when $H=0$ (Ref. 1) and to α in a strong magnetic field, as follows from Eqs. (8), (9), and (26). The transition from the dependence on α^3 to the dependence on α is associated with the participation of free electron–hole pairs as the first N or $N-1$ intermediate states, since their volume in the 3D case is proportional to α^{-3} when $H=0$ and to α^{-1} in a strong magnetic field due to the quasiuniform character of their motion.

The sharp increase in the multiphonon resonant Raman scattering efficiency in the presence of a strong magnetic field unquestionably also applies to ranges b and a (see (34)) of the frequency ω_l below the excitonic resonance point, although the description of multiphonon resonant Raman scattering in these regions requires a calculation of the exciton distribution function $P_{\text{exc}}(K_\perp,|K_z|)$ in a strong magnetic field with consideration of the interaction with acoustic phonons, which, as far as we know, has not yet been performed. However, it is clear that $P_{\text{exc}}(K_\perp,|K_z|)$ is proportional to the creation probability of real excitons with a kinetic energy in the range from zero to $\hbar\omega_{\text{LO}}$, and this probability increases by a factor of α^{-2} in the presence of a strong magnetic field.[2] Therefore, according to (1) and (2), the intensity of the multiphonon resonant Raman scattering below the excitonic resonance point also increases by a factor of α^{-2}.

Measuring the Nth-order multiphonon resonant Raman scattering efficiency as a function of ω_l near the excitonic resonance, we should obtain a curve that is asymmetric about the point $\omega_s=\omega_{1H}$, since passage through this point should be accompanied by an increase in the contribution of the diagram of Fig. 1(b) due to the sharp decrease in the reciprocal lifetime of the real exciton, $\gamma_{\text{exc}}\to\Gamma_{\text{exc}}$ (see (26)), and the appearance of contributions of additional diagrams with the participation of acoustic phonons.

Measuring the dependence of the multiphonon resonant Raman scattering efficiency on the magnetic field strength H, we should obtain maxima at the values of H (44) corresponding to the direct creation of electrons and holes by the exciting radiation near the bottoms of the Landau bands.

I.G.L., V.I.B., and S.T.P. thank the European Community and the Spanish Ministry of Education and Science (DGICYT) for financial support, as well as the University of Valencia for its hospitality. This work was partially supported by DGICYT Grant No. PB93-0687.

This research was performed with partial financial support from the Russian Fund for Fundamental Research

(Grants Nos. 96-02-17115-a and 95-02-04184-a) and the "Physics of Solid-State Nanostructures" Program (Grant No. 1-009).

[1)]The diagram technique that we used is a modification of the well-known technique developed by Keldysh[4] for nonequilibrium processes.

[2)]When $a_H^2 K_\perp^2 \simeq a^2/a_H^2$ the exciton ceases to exist in a strong magnetic field (a is the radius of the exciton when $H=0$), but since the values $x \leqslant 1$ in the integral over x on the right-hand side of (26) are real, it can be assumed that x varies from zero to infinity.

[3)]The distribution function $P_{\text{exc},N}(K_\perp, |K_z|)$ is defined as the number of excitons formed upon emission of N phonons normalized to one photon of exciting light.

[1]V. I. Belitsky, A. Cantarero, S. T. Pavlov *et al.*, Phys. Rev. B **52**, 11 920 (1995).

[2]I. G. Lang, S. T. Pavlov, and A. V. Prokhorov, Zh. Éksp. Teor. Fiz. **106**, 244 (1994) [JETP **79**, 133 (1994)].

[3]L. P. Gor'kov and I. E. Dzyaloshinskiĭ, Zh. Éksp. Teor. Fiz. **53**, 717 (1967) [Sov. Phys. JETP **26**, 449 (1968)].

[4]L. V. Keldysh, Zh. Éksp. Teor. Fiz. **47**, 1515 (1964) [Sov. Phys. JETP **20**, 1018 (1965)].

[5]V. I. Belitsky, M. Cardona, I. G. Lang, and S. T. Pavlov, Phys. Rev. B **46**, 15 767 (1992).

[6]I. G. Lang, S. T. Pavlov, A. V. Prokaznikov, and A. V. Goltsev, Phys. Status Solidi B **127**, 187 (1985).

[7]E. F. Gross, S. A. Permogorov, and V. V. Travnikov, J. Phys. Chem. Solids **31**, 2595 (1970).

[8]R. Planel, A. Bonnot, and C. Benoit à la Guillaume, Phys. Status Solidi B **58**, 251 (1973).

[9]K. Trallero Giner, O. Sotolongo Costa, I. G. Lang, and S. T. Pavlov, Fiz. Tverd. Tela (Leningrad) **28**, 2075 (1986) [Sov. Phys. Solid State **28**, 1160 (1986)].

[10]K. Trallero Giner, O. Sotolongo Costa, I. G. Lang, and S. T. Pavlov, Fiz. Tverd. Tela (Leningrad) **28**, 3152 (1986) [Sov. Phys. Solid State **28**, 1774 (1986)].

Translated by P. Shelnitz